

Glueballs from 1 + 1-dimensional Gauge Theories with Transverse Degrees of Freedom

F. Antonuccio and S. Dalley

Department of Physics, Theoretical Physics
1 Keble Road, Oxford OX1 3NP, U.K.

Abstract

We study 1 + 1-dimensional $SU(N)$ gauge theories with adjoint scalar matter representations, based on a dimensional truncation of 2 + 1 and 3 + 1-dimensional pure QCD, which approximate the dynamics of transversely polarized gluons. The glueballs are investigated non-perturbatively using light-front quantisation, detailed spectra and wavefunctions being obtained for the large- N limit. In general there is some qualitative agreement of the spectra with lattice Monte Carlo data from the higher dimensional QCD. From the light-front wavefunctions we calculate (polarized) structure functions and interpret the gluon and spin content of glueballs. We discuss the phase structure of the reduced theories in relation to matrix models for relativistic non-critical strings.

1 Introduction

While there is little doubt that Quantum Chromodynamics [1] provides a correct description of most high energy processes inside hadrons, our ability to determine its predictions for low energy properties, such as spectrum and wavefunctions, is however much weaker. Of critical interest are the hadrons with excited gluonic modes, glueballs, and hybrid mesons, whose existence is currently amenable to concerted experimental investigation for perhaps the first time. QCD has often been studied in $1+1$ dimensions, especially in the generalization to an infinite number of colours $N \rightarrow \infty$, beginning with 't Hooft [2]. The reasons for doing this are both kinematical and dynamical. Phase space in two dimensions is smaller and therefore simpler. Also many of the characteristic features of hadrons, which are known or expected to arise from highly quantum dynamical effects in $3+1$ -dimensional QCD (QCD₄), materialize as classical or mildly quantum properties in QCD₂. Since there is no angular momentum in one space dimension, conspicuously absent, however, are any features of QCD₄ which rely on transverse degrees of freedom. In particular there are no gluons at all. Is it therefore possible to embellish QCD₂ so as to include some (discrete) remnant of transverse fields without unduly complicating the theory? In this paper we will study in light-front formalism the glueball boundstates of a $1+1$ -dimensional gauge theory based upon a (classical) dimensional reduction of pure QCD₄, a model of gluons which retains all polarizations of these particles but restricts their 3-momenta to the form $k = (k; 0; 0)$. The result is QCD₂ coupled to two mutually interacting adjoint scalars, corresponding to the two possible physical polarizations of (massless) gluons in four dimensions. Despite the rather crude approximation of degrees of freedom, our analysis in general can yield qualitative agreement with spectra obtained by lattice Monte Carlo simulations of pure QCD₄. Having said this, our aim here is not to reproduce the numbers of higher dimensional gauge theory exactly, since the reduced theory is not well-suited to this task, but to treat the longitudinal and some of the transverse dynamics precisely. In this respect the non-abelian reduced gauge model in $1+1$ -dimensions seems to capture much of the physics of the higher dimensional theory.

In the late seventies a remarkable attempt was made by Bardeen et. al [3] to compute the glueball spectrum directly from a strong coupling expansion of large- N light-front Hamiltonian lattice gauge theory.¹ However, the expansion scheme ultimately left an effective potential for transverse motion which had to be determined empirically. Our calculation, based upon the dimensional reduction mentioned above, is formally similar, but obviously does not include transverse kine-

¹Review of more recent approaches to solving four-dimensional light-front gauge theories with further references can be found for example in ref.[4].

matics, which would require knowledge of this effective potential. In order to partially overcome the effects of this omission it is expedient to allow certainly one, and possibly two, adjustable parameters in the reduced theory, which are allowed by $1+1$ -dimensional gauge invariance as we shall see. The analysis we perform is a natural extension of more recent work on the spectrum of adjoint matter in $1+1$ -dimensional large- N gauge theories [5]. The simpler dimensionally reduced model of QCD_3 at large- N has been studied in ref.[6], questions relevant to the Hagedorn behaviour (of adjoint fermions) in refs.[7], and the heavy particle potential in ref.[8]. In this paper we will first perform in more detail the broad spectrum analysis of refs.[5, 6] in order to elucidate the implications for glueballs in QCD_3 , for which there is some preliminary lattice data [9].

Our computations are performed in the large- N limit, which still however allows the number of gluons to fluctuate, unlike the case for quarks. This is done both for practical reasons, in order to keep the Hilbert space small enough to be manipulated on a workstation when studied numerically, and also possibly for reasons of principle in order to avoid subtleties of vacuum structure. The approach we use is analogous to the original one of 't Hooft [2] i.e. naive light-front quantisation in light-front gauge. While this is not in general good enough for studying vacuum properties, such as the value of condensates, it appears to be sufficient for the excitation spectrum.² To solve the boundstate problem numerically we employ discretised light-front quantisation [11, 12] conveniently implemented in terms of a Lanczos algorithm, described in an appendix. We check the numerical results analytically in a phase space wavefunction (PSW) approximation. The solutions yield a mass spectrum and also light-front wavefunctions from which virtually any structure function of interest can be extracted.

The organisation of the paper is as follows. Section 2 introduces the light-front dimensionally reduced model. New numerical and analytic solutions of the boundstate equations for the reduced model of QCD_3 are described in section 3 and compared with the available lattice data. Following the physical lessons learned from this, a similar analysis is applied to the reduced model of QCD_4 in section 4; the glueball boundstate spectrum is compared with lattice data and the structure functions are investigated. In section 5 we briefly look at the phase structure of the reduced model in more detail, particularly in relation to matrix models of string theory which have been studied in a similar light-front formalism [13, 14]. Finally, section 6 summarises the physical conclusions we draw from this work about non-perturbative QCD . Descriptions of the numerical procedures are as far as possible collected in the appendix. An extension of the results to mesons and hybrids is treated in [30].

²For a careful treatment of these questions see for example [10, 28].

2 Dimensional Reduction.

We start from $SU(N)$ Yang-Mills theory in D dimensions

$$S = \frac{1}{4g^2} \int d^D x \text{Tr} F_{\mu\nu} F^{\mu\nu}; \quad (1)$$

$$F_{\mu\nu} = \partial_\mu A_\nu - \partial_\nu A_\mu + i[A_\mu, A_\nu]; \quad (2)$$

and choose light-front co-ordinates $x^\pm = (x^0 \pm x^{D-1})/\sqrt{2}$ and light-front gauge $A_- = 0$. In this case

$$S_{\text{LF}} = \frac{1}{g^2} \int d^D x dx^+ dx^\perp \text{Tr} \left[\frac{1}{2} (\partial_+ A_\perp)^2 + A_+ J^\perp - \frac{1}{4} F_{\perp\mu} F^{\perp\mu} \right]; \quad (3)$$

$$J_{ij}^+ = i[A_\perp^i, A_\perp^j] - \partial_+ A_{ij} - \partial_i A_j + \partial_j A_i; \quad i, j = 1, \dots, N; \quad i, j = 1, \dots, D-2; \quad (4)$$

Repeated indices are summed. The field A_+ is a constrained variable which does not propagate in light-front time x^+ , leaving only the transverse gluons A_\perp as physical degrees of freedom. Much of the complexity of gauge theory is due to the linear term in the longitudinal momentum current (4), so one might as an approximation study the theory truncated to zero modes $\partial_+ A = 0$ only. This is the same as beginning with a $1+1$ -dimensional adjoint gauge theory

$$S_R = \int dx^+ dx^\perp \text{Tr} \left[\frac{1}{2} D_\perp^2 A_\perp^2 - \frac{1}{4g^2} F_{\perp\mu} F^{\perp\mu} - \frac{tg^2}{4} [A_\perp^i, A_\perp^j]^2 \right]; \quad i, j = 1, \dots, N; \quad (5)$$

where $g^2 = g^2 = \int d^D x, D_\perp^2 = \partial_\perp^2 + i[A_\perp^i, \partial_i]; \quad \partial_\perp^2 = \partial_\mu^2 - \partial_+^2$, and $t = 1$. S_R inherits a subgroup of the Poincare and gauge symmetries of the D -dimensional theory. The residual internal symmetries of S_R resulting from gauge invariance of S are just the $1+1$ -dimensional gauge symmetries

$$A_\perp \rightarrow U A_\perp U^\dagger + i(\partial_\perp U) U^\dagger; \quad U \rightarrow U; \quad (6)$$

Due to the asymmetry of the dimensional reduction procedure, which singles out one spatial direction, it is appropriate to allow different longitudinal and transverse gauge couplings. Hence we take t in (5) to be a free parameter, which is still consistent with the reduced gauge invariance (6). In fact the potential for transverse fields in S_R is the only quartic gauge invariant term with the centre symmetry $U(1) \rightarrow \text{const}$. Higher order interactions are not suppressed on dimensional grounds, but neither are they required for renormalisability; in the interests of simplicity we will therefore use the action S_R . It acquires the $SO(1,1)$ subgroup of $SO(D-1,1)$ Lorentz symmetries of S and also has discrete symmetries: charge conjugation $C (A_{ij} \rightarrow -A_{ji})$ induces

$$C : A_{ij} \rightarrow -A_{ji} \quad (7)$$

on the $1+1$ -scalars; there also remains the one-dimensional parity

$$P_1 : x^{D-1} \rightarrow -x^{D-1} ; \quad (8)$$

nally there are the internal symmetries under exchanges of the index which, together with P_1 , form a remnant of the $SO(D-1)$ spatial rotations.

Analysing the boundstates of S_R by light-front quantisation, and taking the large- N limit with $g^2 N$ fixed, results in additional simplifications. The calculation is similar to, but much richer than, the one performed by 't Hooft for the quark-anti-quark pair [2]. The calculation is richer since, unlike the fundamental representation for quarks, any number of adjoint particles may be involved in the formation of a boundstate. With x^+ as canonical time, the A_+ field can be eliminated by its constraint equation to yield canonical momenta:

$$P^+ = \int dx \text{Tr} [\mathcal{E}^2] ; \quad (9)$$

$$P = \frac{g^2}{2} \int dx \text{Tr} \left[\frac{1}{2} [E_i, E_j]^2 + J^+ \frac{1}{\mathcal{E}^2} J^+ \right] ; \quad (10)$$

and the zero-charge condition $\int dx J^+ = 0$, where $J^+ = i[E_i, E_j]$. As in the 't Hooft model, the latter condition restricts one to the space of singlet states under x^- -independent gauge transformations, whose masses are gauge invariant. Quantising on the null line $x^+ = 0$,

$$[E_{ij}(x); E_{kl}(x)] = \frac{1}{2} i (x_i x_k - x_j x_l) \epsilon_{ijlk} ; \quad (11)$$

the boundstate problem reduces to the solution of the mass shell condition,

$$2P^+ P_{-j} |j\rangle = M^2 |j\rangle ; \quad (12)$$

which, for a suitable basis diagonal in P^+ , is a Schrodinger equation for the light-front hamiltonian P_- . Such a basis is formed by the fourier oscillator modes a^y ;

$$|ij(x^+ = 0)\rangle = \frac{1}{2} \int_0^1 \frac{dk^+}{k^+} a_{ij}(k^+) e^{ik^+ x} + a_{ji}^y(k^+) e^{ik^+ x} ; \quad (13)$$

$$[a_{ij}(k^+); a_{jk}^y(k^+)] = (k^+ - k^+) \epsilon_{ijlk} \quad (14)$$

These create the light-front Fock space by action on a particle-free vacuum $a(k^+) |0\rangle = 0$. We will often drop the superscript on k^+ for clarity and refer to it as momentum (it equals k^0 in the traditional infinite momentum frame). Due to the zero charge constraint and the large- N limit the light-front wavefunctions one needs to consider are the set of singlet states of the form

$$|j(P^+)\rangle = \int_{n=2}^1 \frac{dx_1 \dots dx_n}{2} \int_{m=1}^N \frac{dk_m}{k_m} P^+ \frac{f^{1 \dots n}(k_1, \dots, k_n)}{N^{n-2}} \text{Tr} [a_{11}^y(k_1) \dots a_{nn}^y(k_n)] |0\rangle ; \quad (15)$$

For $SU(N)$, $\text{Tr}[\] = 0$, and the one-gluon state is absent. The glueballs (15) may be pictured as a superposition of rings of flux created by a closed chain of n gluons with momenta $k_1; \dots; k_n$. The states with more than one Trace, which are decoupled from these stable flux rings when $1=N \rightarrow 0$, correspond to multiple glueball combinations and may be neglected. Explicit oscillator expressions may easily be obtained for P [5].

The main objective of this paper is to solve (12) for $D = 3$ and $D = 4$, and to explore the consequences. The elementary interaction processes occurring at order g^2 are shown in Figure 1, the principal difference between $D = 3$ and 4 being the absence of the four-gluon transverse-magnetic t -terms in the former case (g.l(c)). We shall see that this difference has significant consequences for the accuracy of valence gluon approximations and the phase structure of the theory. In the large- N limit these processes must form Feynman diagrams that can be drawn on a cylinder, whose ends are the flux rings (15), rather than a strip as in the case of quarks. The only renormalisation which needs to be dealt with in the two-dimensional theory concerns the self-energies shown in g.l(a). There is no transverse gauge invariance to prevent the generation of masses for the fields and so a mass counter-term must be added to S_R if masslessness were to be maintained at the quantum level. In fact, as in the t'Hooft model, the most divergent part of the self-energy is cancelled by zero momentum A_+ -exchange (E -term in g.l(b)) when two or more gluons are present. We elaborate these observations in the specific cases to follow.

3 Reduced QCD₃.

3.1 Boundstate Equations.

First we reconsider the reduced model for $D = 3$ [5, 6]. There is only one transverse gluon field, so we drop the index and call $f_{1 \dots n} = f_n$. By substituting the oscillator expressions (13) into P , normal ordering and taking matrix elements, the mass shell condition (12) can be conveniently summarised by an infinite set of coupled Bethe-Salpeter integral equations for the coefficients $f_n(x_1; \dots; x_n)$ of n -gluon Fock states (cyclically symmetric in their arguments);

$$\begin{aligned} \frac{M^2}{g^2 N} f_n &= \frac{m^2}{g^2 N} \frac{1}{x_1} f_n(x_1; x_2; \dots; x_n) + \frac{p}{4} \frac{1}{x_1 x_2} f_n(x_1; x_2; \dots; x_n) \\ &+ \int_0^{x_1+x_2} \frac{dy}{4} \frac{p}{x_1 x_2 y (x_1 + x_2 - y)} fE[x_1; x_2; y] f_n(x_1; x_2; \dots; x_n) \\ &+ (D[x_1; x_2; y] - E[x_1; x_2; y]) f_n(y; x_1 + x_2 - y; \dots; x_n) g \end{aligned}$$

$$\begin{aligned}
& + \int_0^Z dx_1 \int_0^{x_1-y} dz \frac{F[x_1; y; z] + F[z; y; x_1]}{4 p_{x_1 y z} (x_1 - y - z)} f_{n+2}(y; z; x_1 - y - z; x_2; \dots; x_n) \\
& + \frac{F[x_3; x_2; x_1] + F[x_1; x_2; x_3]}{4 p_{x_1 x_2 x_3} (x_1 + x_2 + x_3)} f_{n-2}(x_1 + x_2 + x_3; x_4; \dots; x_n) \\
& + \text{cyclic permutations of } (x_1; x_2; \dots; x_n) ;
\end{aligned} \tag{16}$$

where the functions

$$E[x_1; x_2; y] = \frac{(x_1 + y)(x_1 + 2x_2 - y)}{(x_1 - y)^2} \tag{17}$$

$$D[x_1; x_2; y] = E[x_2; y; x_1] \tag{18}$$

$$F[x_3; x_2; x_1] = E[x_3; x_1; -x_2] \tag{19}$$

correspond to the elementary processes of g.l. In (16) we have switched to the Lorentz-invariant momentum fractions $x_m = k_m^+ / P^+$, which are the Bjorken scaling variables; the two-dimensional light-front gauge theory exhibits exact scaling. The particle has logarithmic and linearly divergent self-energy in 1+1 dimensions as a result of the first diagram in g.l(a). This diagram arises from normal ordering the $J:J$ term in P (10) (the currents J themselves are assumed already normal ordered) and gives an induced mass [6]

$$\frac{1}{2} m_{\text{ind}}^2 = \frac{g^2 N}{4} \int_0^1 \frac{dp}{p} + \frac{g^2 N}{4} \int_0^k dp \frac{k}{(k-p)^2} \tag{20}$$

As in the t'Hooft model, the linearly divergent part of m_{ind}^2 cancels against zero-momentum A_+ -exchange (g.l(b)) between two particles and can be absorbed into the E -term in (16) to make the integrals manifestly finite at the Coulomb pole $x_1 = y$. To the rest of m_{ind}^2 we have added a bare mass in order to leave a finite renormalised mass m in (16). In this paper we will mostly be interested in the massless limit $m \rightarrow 0$, although no pathology would be incurred in choosing any $m^2 > 0$. In this way one can be sure that whatever constituent gluon masses appear to manifest themselves in the spectrum are dynamically generated. (We stress however that agreement with the higher dimensional lattice results can be improved if a constituent mass m is put in by hand.) Note that dimensional reduction of classical pure QCD_3 can be achieved by compactification of one direction to very small radius, but at the quantum level this results in a diverging Debye mass for Polyakov loops [15]. At small radius these loops can be identified with fields and therefore our mass renormalisation prescription is entirely different from the highly compact gauge theory, whose spectrum is quite dissimilar to the uncompactified one [16].

The elementary processes (g.l) for adjoint particles represented in (16) include the Coulomb potential (E integral), which is linear in two dimensions; it would also be present for fundamental

representation particles but with half the strength $g^2 \rightarrow g^2/2$ since an adjoint source has two flux lines attached to it rather than one. In addition in (16) there is a $2 \rightarrow 2$ annihilation channel (D integral) and pair creation and annihilation of gluons (F integral), which are not suppressed by the large- N limit but for low-lying levels are found to be dynamically suppressed to a very high degree [5].

A survey of the broad features of the mass spectrum M^2 resulting from large- N adjoint scalars in two dimensions has been performed in refs.[3, 6]. A massive spectrum of stable glueballs is organised into approximate valence gluon trajectories for low-lying levels, while at higher energies pair creation dominates to give a complicated picture. We have concentrated on the highly structured seven or so lowest states resulting from (16) in order to compare with Monte Carlo results of the (unreduced) lattice QCD₃. Simple approximate analytic solutions may be found to the equations (16) while numerical solutions may be straightforwardly obtained with the help of Mathematica and a workstation. By cutting the interval of allowed momentum fractions $0 < x < 1$ into $x/2$ ($1=K; 3=K; 5=K; \dots$) for some integer K , the problem becomes one of finite matrix diagonalisation (Discretised Light-Cone Quantisation) [17], the continuum limit being achieved by extrapolating $K \rightarrow 1$. We found it useful to employ a Lanczos algorithm in computing and diagonalising the mass matrix M^2 in this way. A Hilbert space of dimension $\sim 10^3$ can be comfortably handled. Details of our numerical work are given in the appendix. In addition to measuring the masses M from extrapolation of finite K calculations to the continuum limit $K = 1$, we also used the (normalised) light-front wavefunctions ψ_j to compute structure functions of these mass eigenstates at fixed cut-off. In particular the quantities

$$g(x) = \langle \sum_{ij} \bar{\psi}_{ij}(x) a_{ij}(x) \psi_j \rangle \quad (21)$$

$$= \int_{x_1=0}^x \int_{x_2=0}^{x_1} \dots \int_{x_n=0}^{x_{n-1}} dx_1 \dots dx_n \sum_{m=1}^{x^n} x_m \int_{x_m=0}^1 \int_{x=0}^{x_m} (x_m - x) \psi_n^2(x);$$

$$\langle n \rangle = \int_0^1 dx g(x); \quad (22)$$

$$1 = \int_0^1 dx x g(x) \quad (\text{momentum sum rule}); \quad (23)$$

give the the number of gluons $g(x)$ with momentum fraction between x and $x + dx$ in a bound-state and the average number of gluons $\langle n \rangle$. These quantities are helpful in trying to match the $1+1$ -dimensional eigentates forming representations of discrete reduced symmetries with the representations J of the full spatial rotation group $SO(2)$ in $2+1$ dimensions. In addition they suggest appropriate analytic approximations.

3.2 Solutions.

The numerical solutions for the reduced $D = 3$ theory are given in Table 1 and illustrated on Figure 2 (some data for fixed K are tabulated in ref.[6]). As in refs.[5, 6] we note that a spectacularly accurate valence gluon approximation is manifested in the light glueballs described by (16). The Coulomb potential, which includes the 2nd term in (16) as well as the E -integral, dominates since it is the only positive definite and singular amplitude. Both the annihilation channel (D) and pair production (F) amplitudes take either sign with roughly equal probability, leading to much cancellation. Physically they are suppressed because the intermediate A_+ 'particle' is non-propagating in light-cone time x^+ , so couples unfavourably to transverse gluon pairs in the boundstate. The same reasoning may be applied to the good valence approximation for QCD_2 with massive quarks at finite N , which has been studied in the same formalism [17]. Therefore the latter is probably not a very good guide to the accuracy of valence approximations for quarks in higher dimensional QCD , where pair production can proceed via transverse gluons.

In labeling the states with their $(P_1; C)$ quantum numbers, a technical problem arises in determining P_1 , which has the effect $x^+ \rightarrow x^-$ on vectors. This symmetry is broken when the momentum fractions x are discretised, since this is equivalent to (anti)periodic conditions on x^- . Under P_1 , momentum fractions of on-shell partons transform as [17]

$$x_m \rightarrow \frac{1}{x_m} \prod_{n=0}^{n-1} \frac{1}{x_{m-n}}; \quad (24)$$

which in general is not of the form (integer) $\times K$; the exception is $n = 2$, in which case it has the effect $x_1 \rightarrow x_2$. Also it is not obvious that eq (24) represents P_1 in the interacting theory, although we found it to be at least an approximate symmetry of the states exhibited in this paper.³ There are various quantitative and qualitative ways of assessing by inspection the effect of P_1 as given by (24) on eigenfunctions at fixed cut-off K . The qualitative one we found particularly useful was to note that in general P_1 transforms Fock states where one gluon carries most of the longitudinal momentum to Fock states where the momentum is shared evenly between all the gluons.

A striking property of g_2 is the almost linear M versus $\langle n \rangle$ trajectory, which continues much further than we have shown and which is approximately repeated before soon becoming diluted by pair production effects at higher mass. Such a trajectory represents 'radial excitation' of the glueball flux loop in the sense that the mass of a state is increased by adding gluons and their attendant flux lines to the ring. The leading radial trajectory shows featureless structure functions (Figure 3) peaked at $1 = \langle n \rangle$, while the higher trajectory exhibits further oscillatory

³After submission of this paper, similar work appeared for $N = 3$ [29], where a fuller discussion of parity can be found.

behaviour analogous to higher 'angular momentum' states. For the latter there is an increased probability of finding an asymmetrical sharing of the momentum between gluons in the glueball.

It is interesting to note that $g(x)$ remains large for $x \rightarrow 0$ in general, as a result of the massless limit $m \rightarrow 0$. In particular the approximately two-gluon states are rather like cosine wavefunctions, which was also found for the low-lying mesons in the 't Hooft model at small quark mass [17]. In the latter case the massless groundstate meson formed from massless quark and anti-quark had a constant wavefunction in phase space $f_2(x; 1-x) = \text{const.}$. In the present case the $CP_1 = ++$ groundstate wavefunction is approximately gluonium

$$|j\rangle = \int_0^1 dx \frac{f_2(x; 1-x)}{N} \text{Tr}[a^\dagger(x) a^\dagger(1-x)] |j\rangle \quad (25)$$

The wavefunction $f_2(x; 1-x) = g(x)$ is not quite constant due to the extra statistics-related contribution $= 4^p \overline{x_1 x_2}$ to its mass in (16), suppressing it at the endpoints; this gives the glueball spectrum its mass gap. The gluonium approximation, where all f_n are set to zero except for f_2 , is equivalent to the problem of scalar fundamental representation matter [18], with $g^2 \rightarrow 2g^2$. The endpoint behaviour is $f_2 \sim x$ for $x \rightarrow 0$ where

$$\cot\left(\frac{1}{2}\right) = \frac{m^2}{2N g^2}; \quad (26)$$

which is important for determining the form of $1=K$ corrections (see appendix). Note that for $m \rightarrow 0$ one has $f_2(x) \rightarrow \text{const} > 0$ as $x \rightarrow 0$. By arguments analogous to those for quarks at finite N [17], we expect this endpoint behaviour to hold true beyond the gluonium approximation.

On the leading radial trajectory the wavefunctions are well-described by constant ones in phase space for most momentum fractions x . Only near $x = 0$, corresponding to large x -separations, do interactions become appreciable. Therefore one can obtain an estimate for those masses by evaluating M^2 in a sub-basis of phase space wavefunctions (PSW) defined by

$$|n\rangle : f_n(x_1; \dots; x_n) = \text{const.}; f_m = 0 \text{ for } m \neq n \quad (27)$$

A straightforward calculation using (16) shows that M^2 is diagonal;

$$M^2 |j_n\rangle = \frac{n(n-1)g^2 N}{4} |j_n\rangle \quad (28)$$

$$g(x) = n(n-1)(1-x)^{n-2}; \quad (29)$$

in fair agreement with the numerical data (table 1). Only the 2nd term on the r.h.s. of eq.(16), $= 4^p \overline{x_1 x_2}$, which is left over from partial cancellation of the processes involving radiation of zero-momentum $A_+ (gs.1(a)(b))$, contributes to the eigenvalue; it is the principal value of the E

integral. Since $M \rightarrow 0$ asymptotically, one could regard it as the contribution to a constituent gluon mass due to longitudinal interactions, or more appropriately as the groundstate energy stored in the flux string between each pair of neighbouring gluons on the flux ring. Practically speaking, the PSW approximation works well because the lowest radial trajectory starts quite a bit lower than the complex higher trajectories.

3.3 Comparison with QCD_3 .

Recent lattice Monte Carlo data for $SU(3)$ glueball masses extrapolated to the continuum limit in three dimensions [9] is given in table 1 for comparison. Finite lattice spacing errors are significantly reduced in three dimensions, so these results can be considered quite reliable. The classification is J^{PC} , where parity P in two space dimensions is taken to be reflection about one axis (e.g. $x^1 \rightarrow -x^1, x^2 \rightarrow x^2$). Particles of non-zero angular momentum J should be degenerate in P -doublets $j\bar{j} \rightarrow j \quad j \rightarrow \bar{j}$. Although we have no way of telling the true strength of breaking of $SO(2)$ rotational symmetry by the dimensionally reduced theory, which reduces it to a Z_2 subgroup, we will attempt to match our states with J^{PC} labels. Firstly we take $P = P_1$. Under 180° rotations $x^1 \rightarrow -x^1$ and $x^2 \rightarrow -x^2$, but although ϕ is a $1+1$ -dimensional scalar, it is the component of a $2+1$ -dimensional vector, so we will assume this induces P_1 and $\phi \rightarrow -\phi$. Since all the states we study are found to be invariant under

$$O : ij \rightarrow ji; \quad (30)$$

which reverses the ordering of gluons around a flux ring, this implies that $CP_1 = (-1)^{j\bar{j} \bmod 2}$, which rules out half the possible states in three dimensions from the very beginning. In fact it removes precisely one of the states from each P -doublet. (We should point out however that states odd under O can of course be constructed, but that they lie consistently much higher in the spectrum.) One is still left with the problem of spin labelling within the set of even and odd spins separately, because in general there will be mixing within each set, i.e. spin 0 mixes with spin 2 etc.. We took the spin label for states of given $(P_1; C)$ on a radial trajectory to be the lowest which has not appeared with the same $(P_1; C)$ on a lower energy trajectory.

Having truncated to zero transverse momentum, the best one could hope for would be to reproduce the correct level ordering of the higher dimensional theory. The mass ratio scale gets expanded in the reduced theory, which one could ascribe to the level mixing as a result of $SO(2)$ -breaking. It is tempting, in this gauge and in this large- N light-front quantisation scheme, to describe the data in terms of a constituent gluon picture. However, in at least one case this is in clear conflict with the $(N = 3)$ lattice data: a 0^{++} state could be interpreted as an orbital

excitation of a 3-gluon groundstate 1^+ ; on the lattice the 0 is the lower state since it couples to the combination $U_P - U_P^Y$ of one Wilson plaquette U_P , while 1^+ requires a longer lattice Wilson loop. In fact table 1 shows that the ($N = 1$) dimensionally reduced spectra in the $C = -1$ sector predict lighter spin 1 glueballs, in disagreement with the 3D lattice. The ordering in the $C = +1$ sector is quite good by comparison. Spin 1's being lower than spin 2's may be due to the mixing of even spins and odd spins amongst themselves since spin 1 is pushed down by mixing with spin 3 etc. Due to the dominant valence content of wavefunctions, it is easy to assess the effects of a non-zero mass m for gluons. Although this would act to shrink the mass ratio scale and push up the spin 1's, it could not produce a lower-lying 0 .

Lattice results also exist for $SU(2)$ when $C = +1$ [9], although states with $C = -1$ do not appear since Wilson loops are unoriented. We also therefore tried to assess the error in extrapolation to $N = 1$ by fitting to the form $M_1 = M_N \text{const} N^2$ for example. The variation is actually quite small and we do not think that finite N corrections are the major source of error, relatively speaking, but that the discrepancies we have found are probably largely of a kinematic nature due to the severity of the truncation and hence the smallness of the residual Z_2 symmetry. Despite some agreement of the data, our P and especially J assignments must be considered as heuristic since mixing is inevitable. In many ways the reduced model of QCD_4 , which is the case of physical interest, is less ambiguous.

4 Reduced QCD_4 .

4.1 Boundstate Equations.

We now consider the reduced model for $D = 4$, for which there are two transverse polarizations. Since all particles are restricted to move in one space dimension it is especially convenient to work in the helicity basis (c.f. eq(13))

$$a^Y = \frac{a_1^Y}{\sqrt{2}} \frac{ia_2^Y}{\sqrt{2}} : \quad (31)$$

Then

$$h = \int_0^{Z_1} dk f a_{+ij}^Y(k) a_{+ij}(k) - a_{ij}^Y(k) a_{ij}(k) g \quad (32)$$

measures the helicity of a state. The glueball mass eigenstates will have definite helicity, since it is a symmetry of S_R , and fall into degenerate pairs of opposite h . In general of course, these will not exhibit the further degeneracies required to make up $SO(3)$ representations, a penalty of throwing away all transverse momenta.

In the helicity basis the light-front momentum and energy (9), (10) read

$$P^+ = \int_0^1 dk k f a_{+ij}^Y(k) a_{+ij}(k) + a_{+ij}^Y(k) a_{+ij}(k) g; \quad (33)$$

$$\begin{aligned} P^- &= \frac{m_{ind}^2}{2} \int_0^1 \frac{dk}{k} f a_{+ij}^Y(k) a_{+ij}(k) + a_{+ij}^Y(k) a_{+ij}(k) g \\ &+ \frac{g^2}{8} \int_0^1 \frac{dk_1 dk_2 dk_3 dk_4}{k_1 k_2 k_3 k_4} (k_1 + k_2 - k_3 - k_4) f(D[k_1; k_2; k_3] + t) a_{+ij}^Y(k_3) a_{jk}^Y(k_4) a_{il}(k_1) a_{lk}(k_2) \\ &+ (D[k_1; k_2; k_3] - E[k_1; k_2; k_3] - 2t) a_{+il}^Y(k_3) a_{lk}^Y(k_4) a_{+ij}(k_1) a_{jk}(k_2) \\ &+ (t - E[k_1; k_2; k_3]) a_{+ij}^Y(k_3) a_{jk}^Y(k_4) a_{il}(k_1) a_{lk}(k_2) g \\ &+ (k_1 + k_2 + k_3 - k_4) f(F[k_1; k_2; k_3] - t) a_{+ij}^Y(k_1) a_{jk}^Y(k_2) a_{+kl}^Y(k_3) a_{il}(k_4) \\ &+ a_{+ij}^Y(k_3) a_{jk}^Y(k_2) a_{+kl}^Y(k_1) a_{il}(k_4) + a_{+il}^Y(k_4) a_{+ij}(k_1) a_{jk}(k_2) a_{+kl}(k_3) \\ &+ a_{+il}^Y(k_4) a_{+ij}(k_3) a_{jk}(k_2) a_{+kl}(k_1)] \\ &+ (F[k_1; k_2; k_3] + t) a_{+ij}^Y(k_3) a_{jk}^Y(k_2) a_{+kl}^Y(k_1) a_{il}(k_4) \\ &+ a_{+ij}^Y(k_1) a_{jk}^Y(k_2) a_{+kl}^Y(k_3) a_{il}(k_4) + a_{+il}^Y(k_4) a_{+ij}(k_3) a_{+jk}(k_2) a_{kl}(k_1) \\ &+ a_{+il}^Y(k_4) a_{+ij}(k_1) a_{+jk}(k_2) a_{+kl}(k_3)] g \\ &+ (a_+ \cdot a_-): \end{aligned} \quad (34)$$

The same set of elementary processes occur (g.l), with helicity conserved at each vertex. A set of integral equations similar to (16) may be derived; in the following the polarization index is now taken as λ , with the properties $\lambda_+ = \lambda_- + 1 = 1$, $\lambda_+ = 0$, etc..

$$\begin{aligned} \frac{M^2}{g^2 N} f_{1 \dots n} &= \frac{m^2}{g^2 N} \frac{1}{x_1} f_{1 \dots n}(x_1; x_2; \dots; x_n) + \frac{1}{4} \frac{1}{x_1 x_2} f_{1 \dots n}(x_1; x_2; \dots; x_n) \\ &+ \int_0^{x_1+x_2} \frac{dy}{4 x_1 x_2 y (x_1 + x_2 - y)} f E[x_1; x_2; y] f_{1 \dots n}(x_1; x_2; \dots; x_n) \\ &+ (D[x_1; x_2; y] + t) f_{1 \dots n}(y; x_1 + x_2 - y; \dots; x_n) \\ &+ (4t - \frac{1}{2} - 3t - E[x_1; x_2; y]) f_{1 \dots n}(y; x_1 + x_2 - y; \dots; x_n) g \\ &+ \int_0^{x_1} dy \int_0^{x_1 - y} \frac{dz}{4 x_1 y z (x_1 - y - z)} \\ &f(F[x_1; y; z] - t \operatorname{sgn}(\lambda_1) \operatorname{sgn}(\lambda)) f_{1 \dots n}(y; z; x_1 - y - z; x_2; \dots; x_n) \end{aligned}$$

$$\begin{aligned}
& + (F[z; y; x_1] + t \operatorname{sgn}(\gamma_1) \operatorname{sgn}(\gamma_2)) f_{1 \dots n}(y; z; x_1 \dots y \dots z; x_2; \dots; x_n) g \\
& + \frac{1}{4 x_1 x_2 x_3 (x_1 + x_2 + x_3)} f(F[x_3; x_2; x_1] + t \operatorname{sgn}(\gamma_1) \operatorname{sgn}(\gamma_2)) \\
& \quad f_{1 \dots 4 \dots n}(x_1 + x_2 + x_3; x_4; \dots; x_n) \\
& + (F[x_1; x_2; x_3] + t \operatorname{sgn}(\gamma_2) \operatorname{sgn}(\gamma_3)) f_{1 \dots 2 \dots 3 \dots n}(x_1 + x_2 + x_3; x_4; \dots; x_n) g \\
& + \text{cyclic permutations of } (x_1; x_2; \dots; x_n) :
\end{aligned} \tag{35}$$

The mass renormalisation proceeds in exactly the same fashion | the only new ingredient is the normal ordering of the t -terms which gives a further logarithmically divergent contribution to m_{ind}^2 | and it is in the form (35) that we discretise the momentum fractions x for numerical computation.

The variable t is considered as a free parameter, which we will adjust to obtain a physically reasonable spectrum. In particular we find that it must be positive in order for the groundstate glueball to be helicity zero.⁴ Unlike in QCD_3 , gluon pair production can now proceed directly from a contact term $g_1(c)$. While it is therefore less suppressed, for a range of t around zero there is still a discernable valence gluon content for light glueballs. If t is too large however, tachyons appear and eventually there appears to be a phase transition; the phase structure is discussed in more detail in section 5. As in section 3, we primarily study the massless case $m = 0$. However we will find once again that there is an expansion of the mass ratio scale in the reduced theory relative to that obtained from the higher dimensional lattice results, which can be mitigated by including a constituent mass by hand.

From the wavefunctions (15) we also calculate both unpolarized

$$G(x) = \frac{\langle \vec{p}_{+ij}^y(x) a_{+ij}(x) + a_{ij}^y(x) a_{-ij}(x) \rangle}{\langle j \rangle} \tag{36}$$

and polarized

$$G(x) = \frac{\langle \vec{p}_{+ij}^y(x) a_{+ij}(x) - a_{ij}^y(x) a_{-ij}(x) \rangle}{\langle j \rangle} \tag{37}$$

⁴This result was also found for the similar transverse plaquette coupling in the light-front hamiltonian lattice gauge theory of ref.[3].

structure functions. As a consequence of no transverse momenta, there is a trivially satisfied helicity sum rule

$$\int_0^1 dx G(x) = h : \quad (38)$$

In higher dimensions these structure functions would also be integrated over transverse momenta up to some scale Q , the evolution with large Q being calculable within perturbative QCD once the function is specified at a given scale. In the present case $Q = 0$ effectively, and we are performing a non-perturbative calculation of (some of) the long-distance properties of boundstates in QCD₄ scarcely known for any hadron, least of all glueballs.

4.2 Solutions.

Results for masses of the seven lightest glueball states at $t = 0.15$ ($m = 0$) are given in Table 2 and illustrated on Figure 4 classified by jh_f^{1C} . For massless gluons $m = 0$ we are forced to choose a relatively small t in order to avoid tachyons, so it is the longitudinal interactions which are still dominant. As expected, the valence approximation is less accurate than for the $D = 3$ reduced model, but is nevertheless manifest. All the states shown are groundstates with respect to their valence gluon content and, with the exception of 0^{++} , exhibit featureless unpolarized structure functions (Figure 5) peaked at $1 < x < 1$. The $x \rightarrow 0$ behaviour is still governed by eq.(26). The negative P_1 -parity state 0^{+-} , like the 0^{+-} for $D = 3$, has strong longitudinal interactions, which is why it appears relatively heavy. We attribute the persistence of valence gluon dominance to the energy required to add extra flux lines (one per gluon) to the ring, since the study of purely longitudinal interactions in section 3 showed that each contributes roughly $\frac{1}{g^2 N} \approx 8$ to the mass.

Once more, it is possible to estimate the light spectrum in the PSW approximation by setting

$$f_{1 \dots n}(x_1; \dots; x_n) = \text{const} : \quad (39)$$

for a given set of gluon helicities $1; \dots; n$. This provides a sub-basis of wavefunctions $1 \dots n$ for the 'radial' excitations of the groundstate in each jh_f sector ($P_1 = +$). The integrals appearing in the Bethe-Salpeter equations (35) can be done exactly for (39) resulting in a finite M^2 matrix for finite maximum n . Note that M^2 is now no longer diagonal in each sector due to the t -terms. Diagonalising in the sub-basis of PSW's up to $n = 6$ gives the estimates shown as M_{PSW}^2 in table 2. As an example we show the M^2 sub-matrix in the PSW basis $f_{++}; f_{+-}; f_{-+}; f_{--}; g_{++}; g_{+-}; g_{-+}; g_{--}$:

$$\begin{array}{ccccccc}
0 & \frac{1}{2} & (1-t) & 2 & \frac{1}{6}t & 4 & \frac{1}{3}t & 0 & 0 & 1 \\
\vdots & \frac{1}{2} & \frac{1}{6}t & 3 & \frac{1}{2}(1-t) & \frac{3}{2}t & \frac{3}{2}t & 0 & 0 & \vdots \\
& 4 & \frac{1}{3}t & \frac{3}{2}t & 3 & \frac{1}{2}(1-2t) & 0 & 0 & 0 & : \\
& 0 & 0 & 0 & 0 & \frac{1}{2}(1+t) & 0 & 0 & A \\
& 0 & 0 & 0 & 0 & 0 & 3 & 2 & &
\end{array} \quad (40)$$

Polarized structure functions of $h = 0$ glueballs are identically zero while that of the $h_j = 2$ state follows closely the unpolarized function because the non-valence content is small. The spin structure of the $h_j = 1$ state is perhaps the most interesting since it is the nearest thing to a 'nucleon' in the spectrum. Its larger non-valence content means that the unpolarized function is peaked at noticeably smaller x than the polarized one, gluon pairs, which are preferably created at small x , having to be produced with opposite helicity. In Figure 6 we plot the helicity asymmetry $A = G/G$ for the 1^+ glueball. The PSW approximation would give $A(x) = 1/3$. At small x one finds $A(x) < 1/3$ so the helicity tends to be more disordered, while at large x one has $A(x) > 1/3$. In real nucleons one expects $A \rightarrow 1$ as $x \rightarrow 1$ [19] (helicity retention) i.e. a parton carrying most of the momentum also carries most of the helicity. Although this question has presumably not been asked of glueballs before, it does not seem to happen in the reduced model for $t = 0.15$, at cut-off up to $K = 13$ at least, although the $x = 1$ intercept of A does increase with t . Perhaps this an indication that the strength of transverse interactions we are forced to consider at $m = 0$ are too small to accurately reflect the higher dimensional theory.

4.3 Comparison with QCD_4 .

Lattice Monte Carlo simulations of the (quenched) glueball spectrum have been relatively rare and are still crude for all but the lightest state (see e.g. refs.[20, 21, 22]). We used the $SU(3)$ results of ref.[22] for comparison with the large- N reduced model since they include a range of light states. However that computation was performed at fixed lattice spacing ($\beta = 6.4$ on a 32^4 lattice) so one must bear in mind that significant variations in mass ratios are possible when extrapolated to the four-dimensional continuum limit; furthermore, no 'radial' excitations were computed. It is generally believed that $N = 3$ is large in the sense that there is little qualitative difference between $SU(2)$ and $SU(3)$ spectra. Lorentz invariance was restored in the lattice results to the extent that a full J^{PC} classification was possible, but this is clearly not the case in the reduced model, where h^{PC} are the exact quantum numbers. As in the $D = 3$ reduced model, some of the components of given light spin J are pushed higher in spectrum, although each light spin J does seem to be represented by its largest $|j_z|$ values (compare helicity h with spin J in Table 2). In particular the

reduced model does not seem to cope well with states odd under $O : ij \rightarrow ji$, which are needed to make up components with $C = (-1)^{j_z j_{\text{mod} 2}}$ (e.g. $J_z = -1$ for $J^{PC} = 2^{++}$). The results of Table 2 also show that mixing between given $h^{P_1 C}$ seems to prevent the degeneracy with $h = 2$ of an $h = 0$ component, which mixes with excitations of the groundstate scalar glueball 0^{++} . Finally we note that P_1 alone seems to be closer to three dimensional parity P , rather than P_1 combined with $!$, since the parity of the lightest spin 1 would be incorrect in the latter case.

Assuming that the h assignments of the reduced model are a good guide to the J assignments in four dimensions, the level ordering is in qualitative agreement with the lattice result, although once again the mass ratio scale is expanded. Our model (with $m = 0$) prefers a heavy 0^{++} , due to strong longitudinal interactions, which we have treated exactly, while the four-dimensional lattice would prefer it to be lighter. It is quite possible that the effects of transverse interactions, of which we have only retained a remnant, and transverse kinematics shrink the mass ratio scale and make the 0^{++} lighter. To illustrate this possibility one can include a constituent mass by hand, which one might regard as generated by the transverse dynamics that the reduced model neglects. In Table 2 we have also given the spectrum at $K = 12$ for a set of parameters $m^2 = 2g^2 N = 5$; $t = 0.5$. The non-zero gluon mass allows us to choose a value for t comparable to the longitudinal interaction strength. The comparison with the ($N = 3$) four-dimensional lattice data shows much closer agreement, although no amount of fudging can cause the degeneracies necessary for restoration of $SO(3)$ rotational symmetries; the transverse kinematics are clearly needed for this to happen. The main effect on the structure functions is to suppress small x partons (c.f. eq 26), the polarization asymmetry A also being modified slightly (fig. 6).

5 Phase Structure and Matrix Models.

In principle there are two adjustable parameters in the reduced model for QCD_4 , the mass m and quartic self-coupling t . In this section, by deriving bounds on M^2 and quantifying K -dependence, we suggest a phase diagram in the $(m^2; t)$ plane and note the analogy with matrix models of non-critical string theory. As is well known, the planar Feynman diagrams for the field theory of a hermitian matrix ϕ_{ij} with action

$$S = \int d^d x \text{Tr} (\phi^2)^2 + \frac{t}{4N} \phi^4 \quad (41)$$

define a certain type of random surface embedded in D dimensions [23], essentially a discretisation of Polyakov's continuum path integral formulation [24]. Such theories have been analysed for $d = 2$ and $N = 1$ in light-front formalism [13, 14] in very much the same way as the two-dimensional

adjoint gauge theories. The action (41) is merely ungauged. The critical value of β beyond which perturbation theory diverges | individual normal-ordered planar diagrams are UV finite | manifests itself in light-front formalism (without zero modes) as the divergence $M^2 \rightarrow -1$ in the spectrum. Such a transition⁵ occurs for the reduced model of QCD₄ also, separating a parton phase with $\langle n \rangle$ finite from a string phase with $\langle n \rangle = 1$.

Firstly, one can prove that the spectrum is unbounded below if $m^2 < 0$ by using the variational wavefunction

$$\int_0^1 dx \text{Tr}[a_+^Y(x) a_+^Y(1-x)] \mathcal{J} > 0 : \quad (42)$$

Secondly, that the spectrum is unbounded from below if t is sufficiently large can be proven with the (discretised) variational state

$$\text{Tr}[a_+^Y(1=K) a_+^Y(1=K) a_+^Y(1=K) a_+^Y(1=K) \dots a_+^Y(1=K) a_+^Y(1=K)] \mathcal{J} > 0 : \quad (43)$$

Therefore the phase diagram is probably as indicated in Figure 7. In principle it is possible that the point A coincides with $m = t = 0$ and that the spectrum is unbounded below for all $t > 0$ when $m = 0$. The $1=K$ -extrapolation curve of the groundstate M^2 shown in the appendix certainly seems to be dropping rapidly. However, although we could not prove it, our experience suggests that unboundedness is unlikely since we could not find a variational wavefunction which proved that $M^2 = -1$ for all $t > 0$ at $m = 0$ | it is certain that M^2 is positive at $t = m = 0$ | while the matrix model analysis makes definite predictions for the K -dependence [14], which can be manifested at quite small K , for the divergences of the string phase;

$$\langle n \rangle = K ; M^2 = K^2 : \quad (44)$$

Our measurements at $t = 0.15$ showed no sign of a linear divergence of $\langle n \rangle$, rather it seemed to converge to 2.06 . However, at $t = 0.45$ for example we find the K -dependence of eq.(44), suggesting that this point is already in the string phase. The precise details at the transitional values of t are difficult to determine at the small values of K with which we are forced to work here, but it would be interesting to know whether there exists a non-critical string regime analogous to that identified in refs.[13, 14]. Another question that we are unable to answer at this stage concerns the role of $k^+ = 0$ modes on the phase structure, since they probably have to be taken into consideration in the string phase for a faithful treatment of the original field theory (5). Finally we note that if our conclusion concerning boundedness were wrong for $m = 0$, one would be forced to introduce a sufficiently large gluon mass m for given t in order to stabilize the spectrum.

⁵The possibility of phase transition in the adjoint gauge theory when contact self-interaction terms are added was already suggested in refs.[25, 5].

6 Conclusions.

Two-dimensional non-abelian gauge theories have proved to be usefully tractable, especially in light-front formalism and the large- N limit. In this paper we have attempted to incorporate some of the transverse degrees of freedom of pure gauge theory in a two-dimensional context. In this way one can investigate the boundstate properties of physical gluons and spin while postponing many of the subtle problems of renormalisation which arise in higher dimensional light-front formalism. Although our asymmetrical truncation of phase space may seem an arbitrary approximation, the highest penalty paid appears to be the lack of Lorentz multiplet degeneracies in the glueball spectrum. Comparison with the lattice Monte Carlo data for both three and four dimensions showed nevertheless that the dimensionally reduced model always produces some components of each light Lorentz multiplet, and in approximately the same level order. The rogue components which do not appear in the light spectrum are states anti-symmetric under the symmetry transformation $A_{ij} \rightarrow A_{ji}$ of the gauge potential; this fact deserves a better understanding. Although one cannot be sure of the significance of the mechanism in higher dimensions, the two-dimensional model simply generates from the longitudinal Coulomb potential what amounts to a constituent gluon mass structure for the spectrum. This is due to the non-zero groundstate energy for the flux string between neighboring gluons in the flux loop. It is weaker than a true gluon mass and so cannot prevent the wavefunction from spreading in x -space when the gluon mass $m = 0$, although there is a mass gap in the spectrum. It was also the origin of a good valence approximation for the $D = 4$ reduced model. Such an approximation is even more evident for the $D = 3$ model in which case pair production must proceed via a non-propagating longitudinally polarized A_+ eld. An improvement in the comparison with the higher dimensional spectrum was noticed when an explicit gluon mass m is included by hand | this might be necessary anyway to bound the spectrum from below | perhaps compensating for neglected transverse dynamics. The light-front structure functions exhibited physically reasonable behaviour in our chosen region of coupling constant space, being quite close to those of a phase space approximation. More interesting will be their content at finite N , which will govern the decay and formation of glueballs, and when quarks are included.

Although many qualitative features of higher dimensional QCD are reproduced by the reduced models, we are sceptical of its use as the basis for a systematically improvable approximation to Lorentz-invariant quantities at the quantitative level as transverse momenta are added. The limit of zero transverse momentum is a very singular one in the quantum theory [15], which we have avoided by reducing at the classical level and treating subsequent undetermined couplings

phenomenologically. Of course we would be happy to be proved wrong in this scepticism! Rather we consider the transverse lattice approach advocated in ref.[3] to be the most promising for quantitative work | a study is currently in progress | whose mathematical structure is virtually isomorphic to the field theories studied in this paper, although the adjoint fields have a different interpretation. Nearly co-linear phenomena in which transverse momenta are small compared to a typical scale, such as high-energy diffractive scattering, may hold the best opportunity for applying the reduced models quantitatively to a bona fide four-dimensional problem. With this in mind, the scattering amplitudes involving the reduced glueballs and mesons [30] are presently under study.

Acknowledgements: We would like to thank I. Klebanov, I. Kogan, J. Paton, and M. Teper for very valuable discussions; M. Teper for making available to us his lattice results before publication; M. Burkardt and B. van de Sande for pointing out confusions in an earlier manuscript. F.A. is supported by the Commonwealth Scholarship and Fellowship Plan (British Council).

APPENDIX.

The Lanczos Algorithm.

The Lanczos algorithm [26, 27] is an iteration method which may be used to determine numerically the eigenvalues and corresponding eigenstates of a finite linear operator. We may summarise the essential ideas as follows: Given a symmetric eigenvalue problem $Au = \lambda u$, we begin by choosing a normalised vector u_1 , and setting the constant b_1 to zero. A sequence of constants a_n, b_n and orthonormal vectors u_n are then generated by the following recursion relations;

$$\begin{aligned} v_{n+1} &= Au_n - b_n u_{n-1}; \\ a_n &= v_{n+1} \cdot u_n; \\ v_{n+1}^0 &= v_{n+1} - a_n u_n; \\ b_{n+1} &= \frac{v_{n+1}^0 \cdot v_{n+1}^0}{v_{n+1}^0 \cdot v_{n+1}^0}; \\ u_{n+1} &= \frac{v_{n+1}^0}{b_{n+1}}. \end{aligned}$$

It is easy to show that the matrix representation of the operator A with respect to the orthonormal vectors u_n is tridiagonal, with a_n and b_n being the diagonal and codiagonal entries respectively. After a given number of iterations, the eigenvalues and eigenvectors of this tridiagonal matrix approximate those of the original operator, with a progressive improvement in precision as the iteration proceeds. A particular feature of this method is that the extreme eigenvalues are readily obtained to high precision after a comparatively small number of iterations. This makes the algorithm especially useful if one is only interested in studying the low-lying states.

In our investigations, the finite linear operators which need to be diagonalised arise from the discretised versions of the integral equations (16) and (35), in which only odd momentum fractions $x_i \in [0, 1]$ are allowed, coupled with the constraint $x_1 + \dots + x_n = 1$. This enables us to replace the functions $f_1, \dots, f_n(x_1, \dots, x_n)$ with a finite number of components

$$g_1, \dots, g_n(m_1, \dots, m_n) = \frac{1}{K^{n-1}} f_1, \dots, f_n\left(\frac{m_1}{K}, \dots, \frac{m_n}{K}\right);$$

where the odd integers m_i satisfy $m_1 + \dots + m_n = K$. Note that this cutoff regulates both momentum and the number of particles. Thus the linear action of the integral equation (35) on the space of functions f_1, \dots, f_n may be represented in the discrete case as a finite constant matrix whose size is determined by the number of independent components $g_1, \dots, g_n(m_1, \dots, m_n)$. For example, if we set $K = 4$, and consider the zero helicity sector of the reduced $3+1$ theory,

⁶Choosing odd multiples gives rise to a faster rate of convergence towards the continuum limit since the endpoint regions of the x -interval $(0,1)$ are better sampled.

the only relevant components are $g_{+-(1;3)}; g_{+-(3;1)}; g_{+-(1;1;1;1)}$, and $g_{+-(1;1;1;1)}$. The corresponding 4×4 symmetric matrix representing the discretised version of the linear action (35) has the explicit form

$$\begin{array}{c}
 0 \\
 \text{Basis}
 \end{array}
 \begin{pmatrix}
 \frac{2}{3} + \frac{16}{3}x & \frac{4}{3}t + \frac{16}{3} & \frac{16}{3} & \frac{4}{3}t \\
 \frac{16}{3} & \frac{4}{3}t & \frac{2}{3} + \frac{16}{3}x & \frac{4}{3}t + \frac{16}{3} \\
 \frac{4}{3}t & \frac{16}{3} & \frac{4}{3}t & \frac{2}{3} + \frac{16}{3}x \\
 \frac{8}{6}t & \frac{4}{3}t & \frac{8}{6}t & 4 + 16x
 \end{pmatrix}
 \begin{array}{c}
 1 \\
 C \\
 C \\
 C \\
 A
 \end{array}
 ; \quad (45)$$

where $x = m^2 = g^2 N$. Diagonalising the above matrix gives the eigenvalues M^2 in units $g^2 N = 1$.

One strategy which may be used to estimate the continuum (i.e. $K \rightarrow 1$) limit of the theory is to calculate these matrices explicitly for increasing values of K , and then to extrapolate the resulting sequence of eigenvalues. Unfortunately, this procedure is severely limited by the rapid growth in the number of independent components $g_{1 \dots n} (m_1; \dots; m_n)$ as K is steadily increased, making it sometimes difficult to provide reliable estimates of the continuum behaviour of the theory. Approximation methods are then necessary if further progress is to be made.

As in a previous investigation [14], we used Sun and Dec-alpha workstations together with Mathematica to implement the Lanczos algorithm outlined earlier | this way is slow but easy to do. This technique enabled the authors to investigate the cases $K = 13$ in the reduced $3+1$ theory and $K = 22$ for $2+1$. Typically, the algorithm requires a judicious choice of initial vector to ensure that the convergence of the low-lying eigenvalues is well behaved and rapid. Owing to the valence-like structure of the low-lying states, a perfectly adequate initial state consists of two or three valence gluons (depending on whether the helicity is even or odd respectively). It is also important that it have definite symmetry under the operators which commute with the light-cone hamiltonian since, as the iteration proceeds, each of the new vectors formed by the action of the light-cone hamiltonian will possess the same quantum numbers as the initial vector. This helps restrict the size of the vector space one needs to work with. We remark that for $K = 12$, the 0^{++} sector consists of approximately 900 linearly independent vectors, while for $K = 13$, the size of the 1^{++} sector is a little over 1800.

In the context of discretised light-cone quantisation, exploiting the advantages offered by the Lanczos algorithm depends crucially on how one implements the method. Typically, a large number of vectors are produced at each stage in the iteration, and so, as the iteration proceeds, the light-cone hamiltonian will repeatedly act on the same vectors. However, this action is far from trivial, and so the procedure rapidly runs into difficulties due to the enormous growth in the number of vectors that need to be dealt with. Therefore, it was necessary to introduce a system of 'pointers' which connect a set of existing vectors with its image under the action of the

hamiltonian. This conveniently eliminates the need to perform the same calculations repeatedly, and dramatically improves the viability of the method.

Extrapolation.

A foolproof method of extrapolating the results of discretised light-cone quantisation to the continuum limit is still lacking. The extrapolation of finite- K calculations to the continuum limit $1/K = 0$ has been discussed in refs.[17]. Errors due to discretisation of the integrals in equations such as (16) begin at $O(1/K)$ due to the Coulomb pole. In addition, endpoint errors lead to dependence upon K (c.f. eq(26)). Thus for the case $m = 0$ one expects the corrections to form a series in $1/K$ and one can fit n data points taken at different K to a polynomial (Richardson extrapolation)

$$M^2 = a_0 + \frac{a_1}{K} + \frac{a_2}{K^2} + \dots + \frac{a_{n-1}}{K^{n-1}}; \quad (46)$$

with a_0 the continuum limit. a_{n-1}/K^{n-1} evaluated at the lowest value of K employed gives an order of magnitude estimate for the error in extrapolating. These are the errors shown in the tables, which are probably underestimated. We illustrate this procedure below with the masses from the $D = 4$ reduced model (section 4) at $t = 0.15$, since the extrapolation is far from straightforward especially for the groundstate in this case. Given the suppression of non-valence gluons, one can increase the maximum value of K attainable numerically by truncating the Fock space to a few gluons (Tamm-Danco approximation), thus enabling a more reliable extrapolation to $K = 1$. Figure 8 illustrates the polynomial fits for $K = 12; 13$ for all states shown in table 2, and also includes the fit for the groundstate obtained from data for $K = 18$ by using the $2; 4; 6$ -gluon sector only (chain line).

References

- [1] H. Fritzsch, M. Gell-Mann, and H. Leutwyler, Phys. Lett. B 47 (1973) 365;
D.J. Gross and F.W. Ilczek, Phys. Rev. Lett. 30 (1973) 1343;
S. Weinberg, Phys. Rev. Lett. 31 (1973) 494.
- [2] G. 't Hooft, Nucl. Phys. B 75 (1974) 461.
- [3] W.A. Bardeen and R.B. Pearson, Phys. Rev. D 14 (1976) 547;
W.A. Bardeen, R.B. Pearson, and E. Rabinovici, Phys. Rev. D 21 (1980) 1037.
- [4] S.J. Brodsky, G.M. McCartor, H.-C. Pauli, and S.S. Pinsky, Particle World 3 (1993) 109.
- [5] S. Dalley and I.R. Klebanov, Phys. Rev. D 47 (1993) 2517.
- [6] K. Demeter, I.R. Klebanov, and G. Bhanot, Nucl. Phys. B 418 (1994) 15.
- [7] G. Bhanot, K. Demeter, and I.R. Klebanov, Phys. Rev. D 48 (1993) 4980;
D. Kutasov, Nucl. Phys. B 414 (1994) 33.
- [8] T.H. Hansson and R. Tzani, Nucl. Phys. B 435 (1995) 241.
- [9] M. Teper, Phys. Lett. B 289 (1992) 115; Phys. Lett. B 311 (1993) 223; and to appear.
- [10] F. Lenz, M. Thies, S. Levit, and K. Yazaki, Ann. Phys. (NY) 208 (1991) 1.
- [11] C.B. Thom, Phys. Rev. D 19 (1979) 639; Phys. Rev. D 20 (1979) 1435.
- [12] H.-C. Pauli and S.J. Brodsky, Phys. Rev. D 32 (1985) 1993 and 2001.
- [13] S. Dalley and I.R. Klebanov, Phys. Lett. B 298 (1993) 79.
- [14] S. Dalley, Phys. Lett. B 334 (1994) 61;
F. Antonuccio and S. Dalley, Phys. Lett. B 348 (1995) 55.
- [15] E.D. Hoker, Nucl. Phys. B 201 (1982) 401.
- [16] A. Ferrando and A. Jaramillo, Phys. Lett. B 341 (1995) 342.
- [17] K. Hombostel, S. Brodsky, and H.-C. Pauli, Phys. Rev. D 41 (1990) 3814;
K. Hombostel, Ph.D. Thesis, SLAC report No. 333 (1988).
- [18] S.S. Shei and H.S.T. sao, Nucl. Phys. B 141 (1978) 445;
M.B. Halpern and P. Senjanovic, Phys. Rev. D 15 (1977) 1655;
T.N. Tomaras, Nucl. Phys. B 163 (1980) 79.
- [19] S.J. Brodsky, M. Burkardt, and I. Schmidt, Nucl. Phys. B 441 (1995) 197.
- [20] C. Michael and M. Teper, Nucl. Phys. B 314 (1989) 347.

- [21] H . Chen et al, Nucl. Phys. (Proc. Suppl.) B 34 (1993) 378.
- [22] G . S. Bali et al, Phys. Lett. B 309 (1993) 378.
- [23] F . David, Nucl. Phys. B 257 (1985) 45;
 V A . Kazakov, I K . Kostov, and A A . Migdal, Phys. Lett. B 157 (1985) 295.
- [24] A M . Polyakov, Phys. Lett. B 103 (1981) 207.
- [25] I R . Klebanov and L . Susskind, Nucl. Phys. B 309 (1988) 175.
- [26] C . Lanczos, J. Res. Natl. Bur. Stand. 45 (1950) 255.
- [27] J R . Hiller, Phys. Rev. D 44 (1991) 2504.
- [28] H -C Pauli, A C Kalloniatis, and S Pinsky, Phys. Rev. D 52 (1995) 1176.
- [29] M Burkardt and B . van de Sande, preprint MPI H-V 38-1995, hep-ph/9510104.
- [30] F . Antonuccio and S . D alley, Oxford preprint OUTP-9548P .

FIGURE and TABLE CAPTIONS

Table 1 - M is the $K = 1$ extrapolated mass in units of $\sqrt{N g^2}$ based upon exact diagonalisations up to $K = 22$. $\langle n \rangle$ is calculated for illustration from the theory truncated to the 2-,4-,6-gluon sector only for $K = 20$, or to the 3-,5- gluon sector for $K = 19$. The heuristic J assignments are discussed in text. The lattice $SU(3)$ masses $M_{SU(3)}$ have groundstate 0^{++} normalised to M and a 2% statistical error estimate (ours).

Table 2 - Exact M^2 in units of $N g^2$ for various K at $m = 0$ and $t = 0.15$; the continuum limit; $\langle n \rangle$ at $K = 12$; $M_m^2 = M^2$ at $K = 12$ for $m^2 = 2g^2 N$ and $t = 0.5$; $\langle n \rangle$ for the latter. Also given are mass squared ratios M^2 to the groundstate. Lattice $SU(3)$ mass squared ratios to the groundstate $M_{SU(3)}^2$ are taken from the calculation of ref.[22] at fixed lattice spacing and are rounded to two figures here.

Figure 1 { The elementary processes contributing at order g^2 in S_R : (a) self-energy; (b) longitudinal interactions; (c) transverse interactions.

Figure 2 { Mass spectrum, in units of $\sqrt{N g^2}$, extrapolated to the continuum limit $K = 1$ and classified by $P_1; C$.

Figure 3 { Gluon structure functions $g(x)$ of glueball mass eigenfunctions. Full lines refer to states on the lower 'radial' trajectory in g^2 and chain lines to the states on the upper trajectory. (a) $\langle n \rangle = 2$; (b) $\langle n \rangle = 3$; (c) $\langle n \rangle = 4$; (d) $\langle n \rangle = 5$.

Figure 4 { Mass squared spectrum in units of $N g^2$ at $m = 0$ and $t = 0.15$, extrapolated to the continuum limit $K = 1$ and classified by J^{PC} (non-zero J are doublets).

Figure 5 { Gluon structure functions $G(x)$ for $m = 0$ and $t = 0.15$

Figure 6 { Polarization Asymmetry $A(x) = G/G$ of the 1^+ glueball at $K = 13$. Dotted line for $m = 0$ and $t = 0.15$, full line for $m^2 = 2g^2 N$ and $t = 0.5$.

Figure 7 { Suggested $(m^2; t)$ phase diagram. The shaded region has unbounded $M^2 \rightarrow -1$, while the theory is non-tachyonic in a neighbourhood of the positive m^2 -axis.

Figure 8 { Polynomial fits to M^2 data (units of $g^2 N$) at $t = 0.15$ and $m = 0$.

Table.1

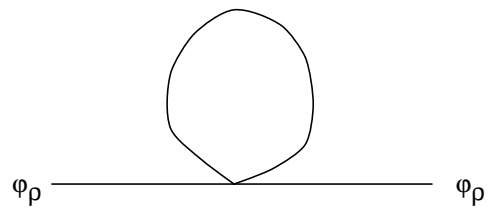
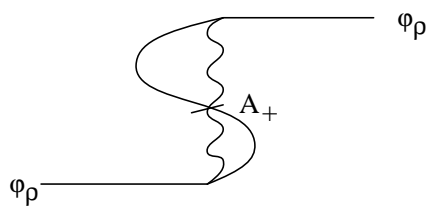
REDUCED							
$P_{1C} (J)$	$++ (0)$	$+(1)$	$++ (0)$	$+(1)$	$++ (2)$	(0)	$++ (0)$
M	2.1 (1)	3.4 (1)	4.7 (1)	5.9 (1)	6.3 (1)	6.6 (1)	7.1 (1)
$\langle n \rangle$	2.002	3.002	4.000	4.990	2.175	3.085	5.902
M_{PSW}	2.2	3.8	5.4	7.0	{	{	8.6
LAT T I C E							
J^{PC}	0^{++}	0^{++}	0	2^{+}	0	0^{++}	
$M_{SU(3)}$	2.1 (1)	3.2 (1)	3.2 (1)	3.5 (3)	4.0 (2)	4.0 (2)	

Table.2

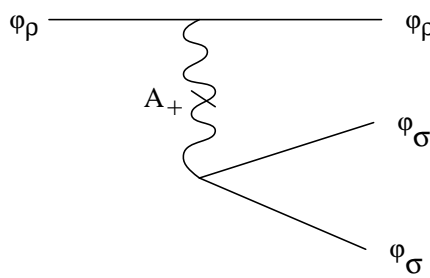
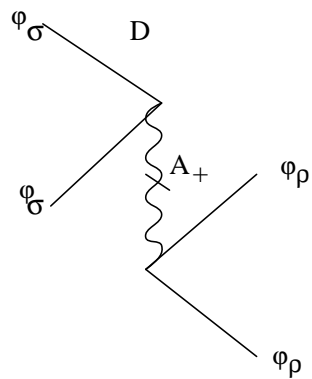
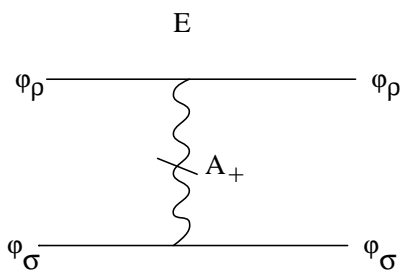
REDUCED							
$h_f^{P_{1C}}$	0^{++}	2^{++}	1^{+}	0^{++}	0^{++}	2^{++}	0^{+}
valence	$a_+ a$	$a a$	$a a a$	$a_+ a a_+ a$	$a_+ a_+ a a$	$a a a a$	$a_+ a$
$K = 6$	3.12186	4.28929	8.78276 ¹⁾	11.453	14.502	14.814	16.1509
$K = 8$	3.24943	4.43805	9.18900 ²⁾	12.303	15.813	16.1555	17.2769
$K = 10$	3.25875	4.53335	9.46014 ³⁾	12.835	16.686	17.0475	18.0253
$K = 12$	3.25605	4.59893	9.65198 ⁴⁾	13.193	17.309	17.6828	18.5584
$K = 1$	3.1 (3)	4.9 (1)	10.7 (2)	14.9 (4)	21.0 (4)	21.3 (9)	21.7 (3)
$\langle n \rangle$	2.062	2.002	3.031 ⁴⁾	4.011	4.021	4.025	2.134
M_{PSW}^2	3.1	5.7	13.3	17.0	27.9	28.6	—
M_m^2	14.56	18.21	37.29 ⁴⁾	—	—	—	35.98
$\langle n \rangle$	2.042	2.005	3.027 ⁴⁾	—	—	—	2.022
M_m^2	1	1.25	2.56	—	—	—	2.47
LAT T I C E							
J^{PC}	0^{++}	2^{++}	1^{+}				0^{+}
$M_{SU(3)}^2$	1	1.5 (1)	1.9 (2)				1.5 (2)

¹⁾ $K = 7$; ²⁾ $K = 9$; ³⁾ $K = 11$; ⁴⁾ $K = 13$

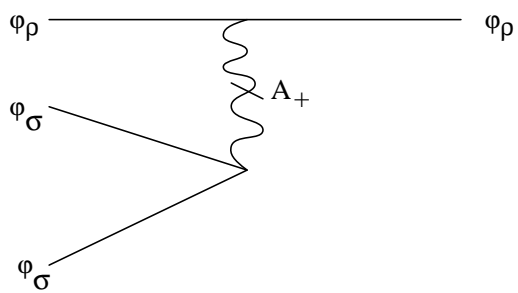
(a)



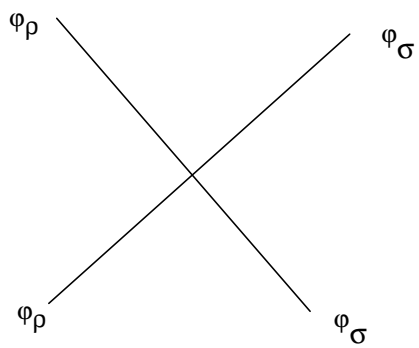
(b)



F



(c)



t

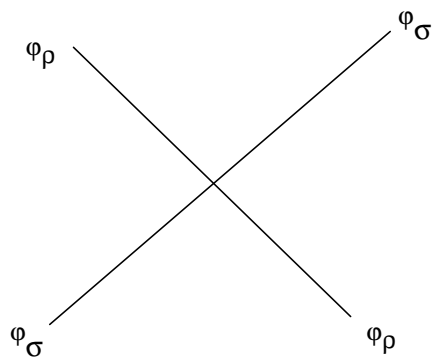


Figure 1

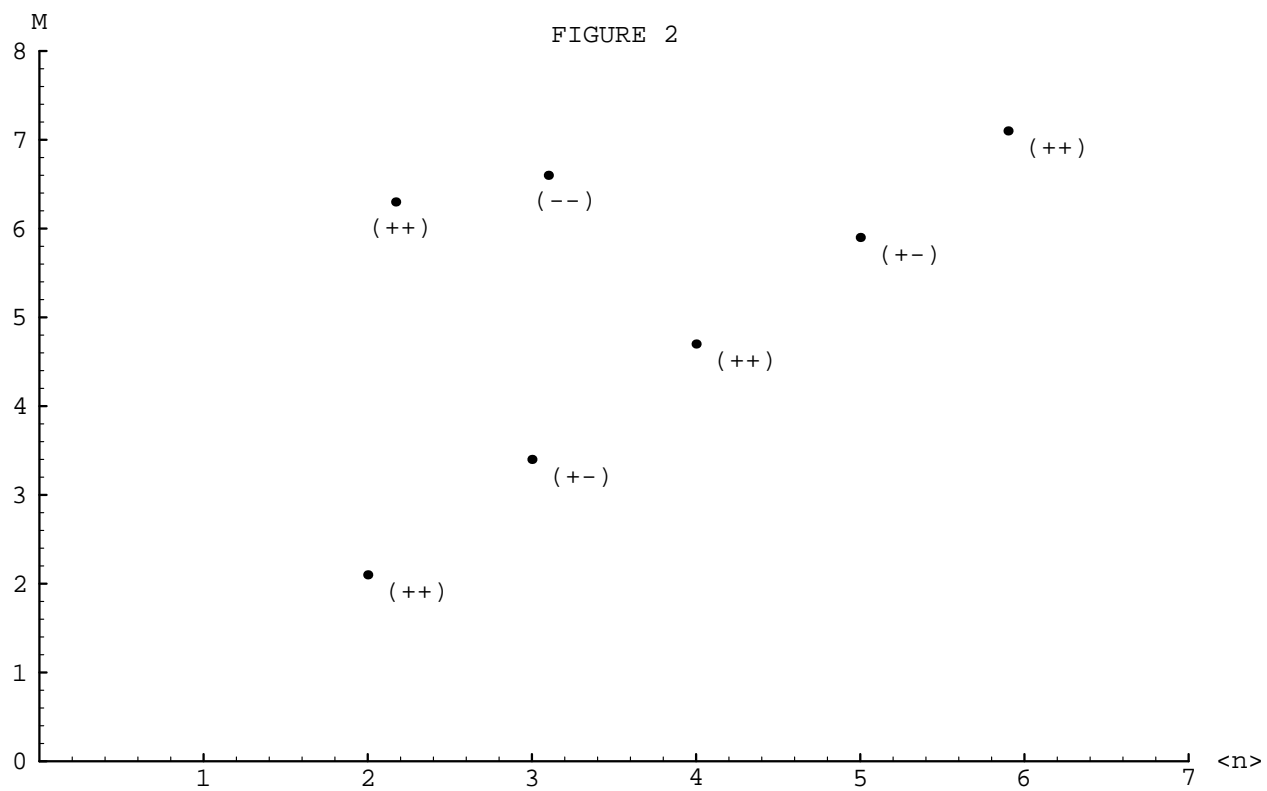
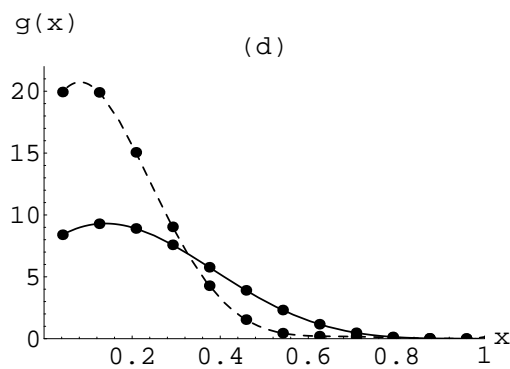
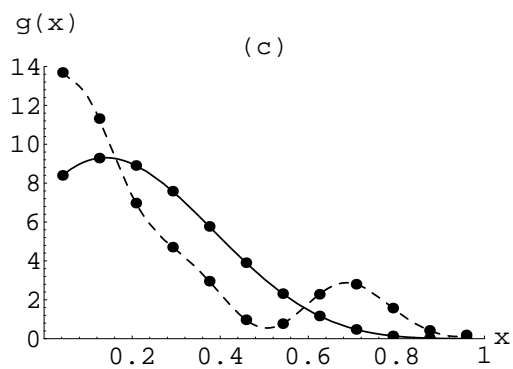
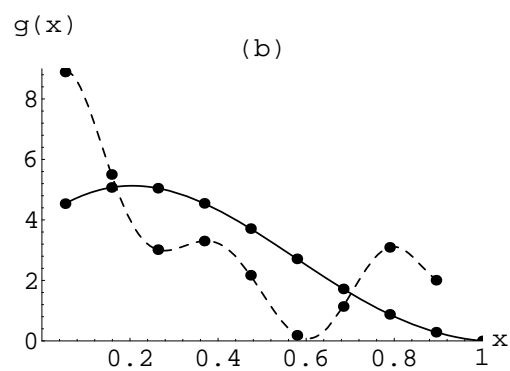
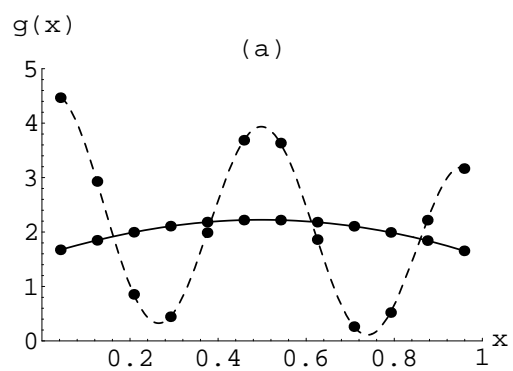


FIGURE 3



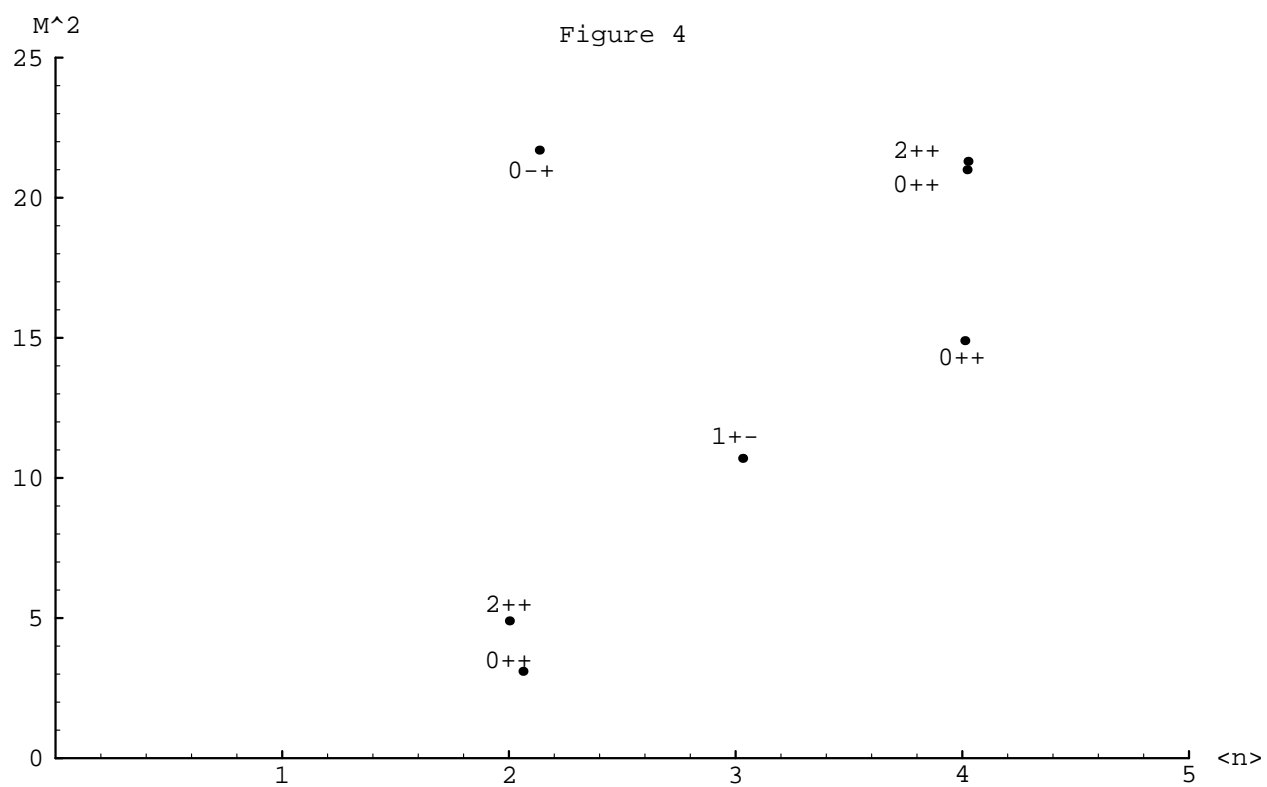


Figure 5

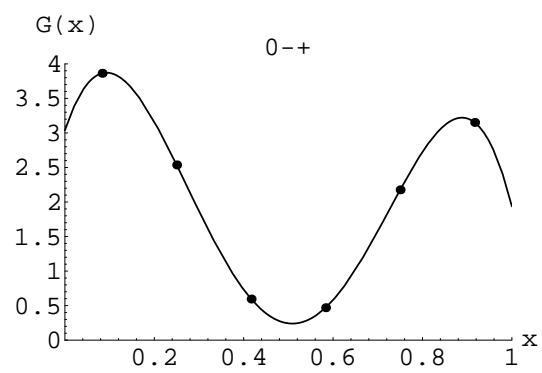
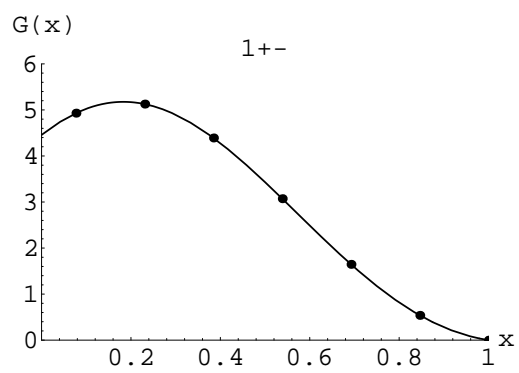
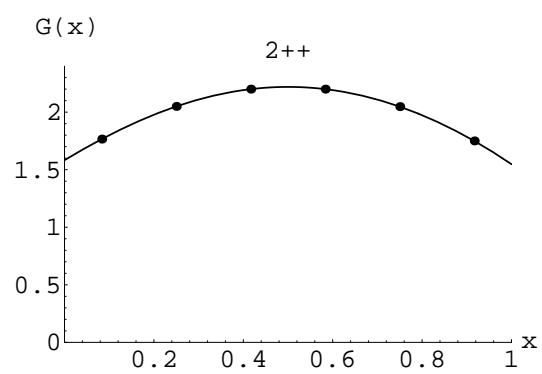
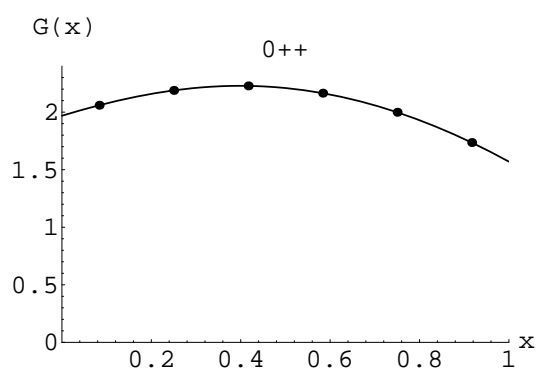


Figure 6

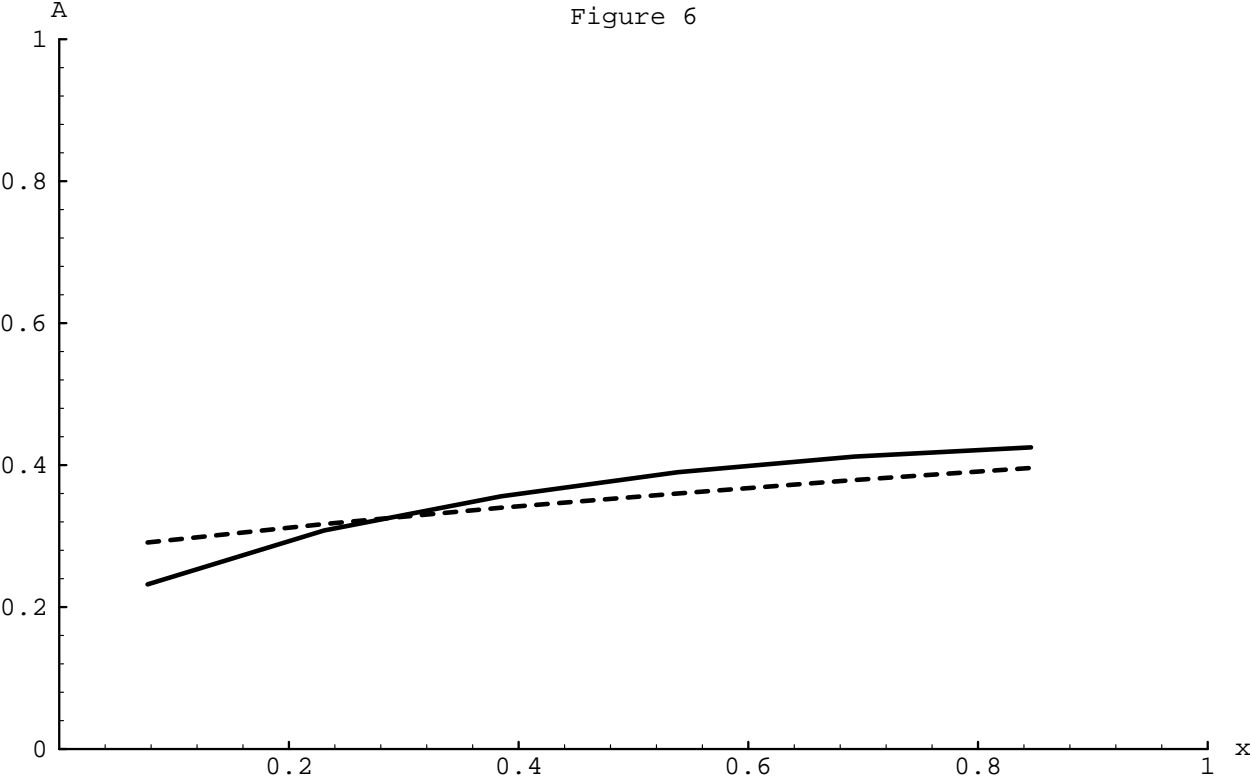


Figure 7

